# Effects of excess pore pressure dissipation on liquefaction-induced ground deformation in 1-g shaking table test

B. Wang[*1], K. Zen[2], G.Q. Chen[2] and K. Kasama[2]

[1]*Graduate Student, Geo-disaster Prevention Laboratory, Department of Civil and Structural Engineering, Kyushu University, Fukuoka 819-0395, Japan*
[2]*Department of Civil and Structural Engineering, Graduate School of Engineering, Kyushu University, Fukuoka 819-0395, Japan*

**Abstract.** Focusing on the effect of excess pore pressure dissipation on liquefaction-induced ground deformation, a series of 1-g shaking table tests were conducted in a rigid soil container by use of saturated Toyoura sand, the relative density of which was 20-60%. These tests were subjected to the sinusoidal base shaking with step increased accelerations: 100, 200, 300 and 400 Gals for 2-4 seconds. Shaking table tests were done using either water or polymer fluid with more viscous than water, thus varying the sand permeability of model tests. Excess pore pressures, accelerations, settlements and lateral deformations were measured in each test. Test results are presented in this paper and the effect of sand permeability on liquefaction and liquefaction-induced ground deformation was discussed in detail.

**Keywords:** liquefaction; lateral flow; settlement; sand permeability; shaking table test.

## 1. Introduction

Due to previous earthquakes, liquefaction-induced lateral flow of sloping ground has extensively damaged lifeline facilities and pile foundations, especially those in ports and harbor structures. For example, the damages were reported typically during the 1964 Niigata earthquake, the 1983 Nihonkai-Chubu earthquake and the 1995 Hyogoken-Nambu earthquake (e.g., Hamada *et al.* 1986, Tohno *et al.* 1986) Such sufficiently large lateral extent may occur even in level deposits.

Recently, several researchers have been studying on the liquefaction-induced ground lateral flow by model tests in 1-g and centrifuge shaking table tests and have given a general picture of how the soil behaviors during liquefaction and lateral flow (e.g., Sasaki *et al.* 1992, Yasuda *et al.* 1992, Hamada *et al.* 1998, Toyota *et al.* 2004, Ikeno *et al.* 2009). By using the knowledge obtained from shaking table tests as well as from past earthquakes, several researchers have proposed the methods to estimate the ground lateral flow empirically or analytically (e.g., Hamada *et al.* 1986, Towhata *et al.* 1999, Shamoto *et al.* 1998).

---

*Corresponding author, Ph.D. Student, E-mail: wangbocumt@gmail.com

The magnitude of ground lateral flow is affected by a number of factors. One of the important factors is the geometry of liquefied subsoil such as thickness of soil layers, slope inclination of ground and boundary conditions. Another important issue is the properties of sands such as the relative density, permeability as well as the duration and frequency of input shaking. Generally, the knowledge about the tendencies of sand to generate and dissipate excess pore pressures during liquefaction is mainly derived from completely undrained tests. Sand underneath a gravity structure, however, behaves neither completely drained nor completely undrained. The effect of permeability can be very significant especially when considering the post-liquefaction residual excess pore pressure and corresponding deformation. Researches that mentioned this issue seem to be quite few (Okamura *et al.* 2001). For this reason, series of 1-g shaking table tests are performed in terms of the permeability effect by using water and polymer fluid. The present text attempts to achieve a detailed discussion about this issue based on the results of those 1-g shaking table tests.

## 2. Outline of test

Fig. 1 shows a schematic rigid soil container which was employed in present 1-g shaking table test, whose dimensions are 80 cm × 30 cm × 70 cm. The front wall of the container was made of glass to observe the deformation of sand layer in the soil container.

Three configurations of model slope were investigated: with 20% inclination, 10% inclination and 5% inclination, respectively. Sloped ground was underlain by a layer of compacted sand which was densified by lightly plunging and the surface soil was trimmed by removing the overlying loose sand. Consequently, the liquefiable sand layer with uniform slope angle and thickness were prepared. During sample preparation, a square grid of noodles and markers were installed along one of the transparent side walls so that the overall deformation of sand layer during shaking table test could be observed visually. Acceleration and excess pore water pressure in soil layers of each shaking table test were measured at the positions as shown in Fig. 1.

Toyoura sand used in this study, was rained down into the container filled with water or polymer fluid to a pre-calculated depth at the relative density $D_r = 20\text{-}60\%$. The specific gravity of the Toyoura sand is 2.644 and its minimum and maximum void ratios $e_{min}$ and $e_{max}$, respectively are $e_{min} = 0.606$ and $e_{max} = 0.977$. Grain size distribution curve of toyoura sand is shown in Fig. 2.
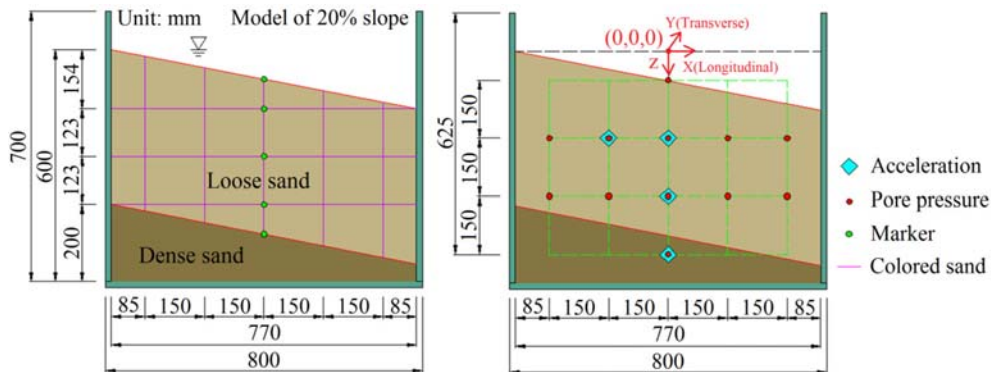


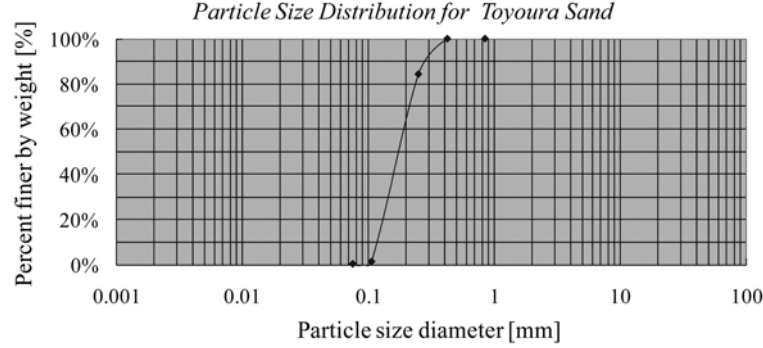Fig. 1 Configuration and measurement of shaking table tests

Fig. 2 Grain size distribution curve of Toyoura sand

The model sand deposits were saturated with either water or with a polymer fluid, which was a mixture of water and polymer materials by weight to achieve a pore fluid with more viscous than water, in order to simulate the prototype sand deposit in model test. The coefficient of permeability in model test was considered to satisfy similarity law in 1g gravitational field. The drainage coefficient, $C$, is a significant factor to dominate the flow in sand

$$C = \frac{c_v}{l^2} \cdot t \tag{1}$$

$$c_v = \frac{k}{m_v \cdot \gamma_w} \tag{2}$$

Where $C_v$ is the coefficient of consolidation, $l$ is the thickness of permeable layer, $t$ is time, $k$ is the coefficient of permeability, $m_v$ is the coefficient of volume compressibility and $\gamma_w$ is the unit weight of pore fluid. The drainage coefficient in prototype is expressed by $C_p$ and that in model test is expressed by $C_m$, and they are respectively represented by

$$C_p = \frac{c_{vp}}{l_p^2} \cdot t_p \tag{3}$$

$$C_m = \frac{c_{vm}}{l_m^2} \cdot t_m \tag{4}$$

It is considered that the similarity law is satisfied when $C_p$ is equal to $C_m$. By setting Eq. (3) equal to Eq. (4), Eq. (5) is obtained as follow

$$\frac{k_m}{k_p} = \left(\frac{t_p}{t_m}\right) \cdot \left(\frac{l_m}{l_p}\right)^2 \cdot \left(\frac{m_{vm}}{m_{vp}}\right) \cdot \left(\frac{\gamma_{vm}}{\gamma_{vp}}\right) \tag{5}$$

The coefficient of volume compressibility is formulated as the following equation

$$m_v = \frac{1}{E} = A \cdot (\sigma_v)^{-n} \tag{6}$$

where $E$ is the young modulus, $A$ is the experimental constant, $\sigma_v$ is effective stress, $n \cong 0.5$ is

Table 1 The law of similitude in shaking table test

| Items | Length | Time | Permeability | Pore pressure | displacement |
|---|---|---|---|---|---|
| Scaling factors (prototype/model) | $\lambda$ | $\lambda^{0.5}$ | $\lambda$ | $\lambda$ | $\lambda$ |
| Value | 8 | 3 | 8 | 8 | 8 |

considered in the model experiment as shown in the geotechnical engineering handbook by the Japanese geotechnical society. The $\gamma_{wm}/\gamma_{wp}$ gives 1, as the density of water is nearly equal to that of polymer fluid. $m_{vm}/m_{vp}$ is represented by

$$\frac{m_{vm}}{m_{vp}} = \left(\frac{\sigma_{vm}}{\sigma_{vp}}\right)^{-0.5} \cong \left(\frac{\gamma_{vm}}{\gamma_{vp}} \cdot \frac{l_m}{l_p}\right)^{-0.5} = \left(\frac{l_m}{l_p}\right)^{-0.5} \tag{7}$$

By substituting Eq. (7) into Eq. (5), we can get

$$\frac{k_m}{k_p} = \left(\frac{t_p}{t_m}\right) \cdot \left(\frac{l_m}{l_p}\right)^{1.5} \tag{8}$$

Iai (1989) has derived a similitude relation with the basic equation governing the equilibrium and mass balance of the soil skeleton, pore water and pile structures. In this study, based on the law of similitude derived by Iai (1989) and Lin *et al.*, (2006), the mass, length and time scale factors can all be expressed in terms of the geometric scaling factor $\lambda = l_p/l_m$ by defining scaling conditions for density ($\rho_p/\rho_m = 1$) and acceleration ($a_p/a_m = 1$) (Iai 1989, Lin *et al.* 2006). The corresponding scaling of parameters between the prototype and model test used in this experiment are listed in Table 1.

The depth of sand deposit in model test is about $l_m = 0.6$ m. So based on the geometric scaling factor, $l_p/l_m = \lambda = 8$, we can get the height of soil layer in prototype $l_p = l_m \cdot \lambda = 4.8$ m. Therefore, the conclusion from those model tests may be restricted to cases in which the depth of liquefied sand layer is about 5 meters. Of course, a greater thickness of liquefiable sand in field situation can be simulated by increasing the dimensions of soil container or the geometric scaling factor $\lambda$ used in model test.
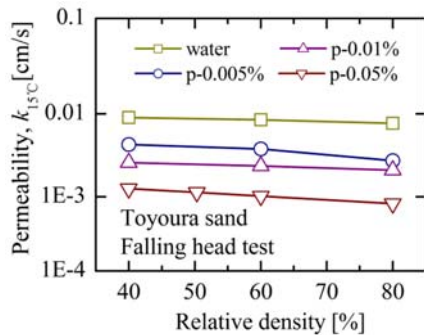


Fig. 3 Permeability of Toyoura sand in water and in polymer fluid at the standard temperature of 15°C
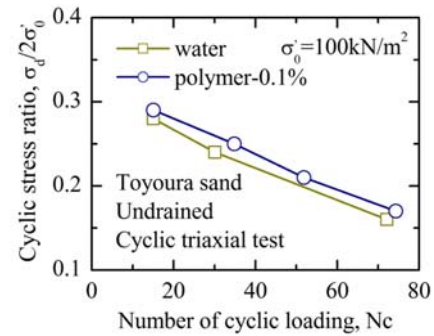
Fig. 4 Liquefaction strength of Toyoura sand in the cyclic triaxial tests (modified after Tomi 2010)

   In this study, the polymer fluid of 0.05%, 0.01%, 0.005% by weight and water were used to change the permeability of sand deposits in model tests. Fig. 3 shows the relationship between relative density and the coefficient permeability of Toyoura sand in water and polymer fluid at the standard temperature of 15 obtained from Falling Head Permeability Tests (JIS A 1218:2009).

   In order to examine whether the polymer fluid affects the mechanical properties of the sand when polymer, such a viscous pore fluid was used, series cyclic undrained triaxial tests were conducted (Tomi 2010). The samples using Toyoura sand were saturated by water and the 0.1% polymer fluid by weight. Fig. 4 shows the results of cyclic triaxial tests. It can be seen that using the polymer fluid has less effect on the mechanical properties of the sand from the point of view on the liquefaction strength. The effect was also discussed by Dewoolkar *et al.* (1999) and came to same conclusions, when he used a Metolose solution in centrifuge model tests. Therefore, it is possible to apply the polymer as the experiment fluid in those tests to determine the permeability of sand deposits. It could be an efficient way to consider the drainage condition of post-liquefaction deformation

Table 2 Tests conditions

| Cases | $H_m$ cm | $\theta$ % | $Dr$ % | $k_{15°C}$ cm/s | $T_m$ s | Liquid W/P | Shaking direction L/T |
|---|---|---|---|---|---|---|---|
| Case 1 | 60 | 0 | 43.4 | 0.0091 | 10 | w | L |
| Case 2 | 60 | 0 | 44.3 | 0.0159 | 2-16 | w | L |
| Case 3 | 60 | 0 | 35.6 | 0.0047 | 2-16 | P-0.005% | L |
| Case 4 | 60 | 0 | 36.9 | 0.0016 | 2-16 | P-0.01% | L |
| Case 5 | 60 | 0 | 50.3 | 0.0011 | 2-16 | P-0.05% | L |
| Case 6 | 60 | 0 | 40.2 | 0.0163 | 2-16 | w | T |
| Case 7 | 60 | 0 | 30.7 | 0.0020 | 2-16 | P-0.05% | T |
| Case 8 | 60 | 0 | 22.6 | 0.0034 | 2-16 | P-0.01% | T |
| Case 9 | 60 | 0 | 18.0 | 0.0054 | 2-16 | P-0.005% | T |
| Case 10 | 40 | 5 | 44.7 | 0.0091 | 2 | W | T |
| Case 11 | 40 | 10 | 22.0 | 0.0097 | 2 | W | T |
| Case 12 | 40 | 20 | 27.5 | 0.0092 | 2 | W | T |
| Case 13 | 40 | 20 | 22.8 | 0.0052 | 2 | P-0.005% | T |
| Case 14 | 40 | 5 | 25.9 | 0.0035 | 2 | P-0.01% | T |
| Case 15 | 40 | 10 | 35.0 | 0.0036 | 2 | P-0.01% | T |
| Case 16 | 40 | 20 | 39.8 | 0.0036 | 2 | P-0.01% | T |
| Case 17 | 40 | 5 | 39.0 | 0.0021 | 2 | P-0.05% | T |
| Case 18 | 40 | 10 | 31.4 | 0.0020 | 2 | P-0.05% | T |
| Case 19 | 40 | 20 | 29.6 | 0.0020 | 2 | P-0.05% | T |
| Case 20 | 40 | 20 | 43.2 | 0.0021 | 2 | P-0.05% | L |

$H_m$: thickness of liquefied layer
$\theta$: inclinationof the ground surface and bottom surface of the liquefied layer
$Dr$: relative density of liquefied layer
$k_{15°C}$: coefficient of permeability of liquefied layer at the standard temperature of 15°C
$T_m$: shaking duration time
W/P: pore fluid, W: water, P: polymer fluid
L/T: shaking direction, L: longitudinal, T: Transverse

in the ground.

To isolate the gravity-induced ground flow along the longitudinal direction of the container from the inertial effects due to shaking, an impulse shaking along the transverse direction for short time duration were applied to the model ground. Flow failure of liquefied ground occurred under a gravity force. For comparison, several test cases were produced by shaking in the longitudinal direction of soil container. The acceleration of shaking was increased step by step loading: 100 Gal, 200 Gal and 300 Gal of 3 Hz. A total of 20 Cases of shaking table tests were conducted under the test conditions as listed in Table 2.

## 3. Effects of soil permeability on liquefaction

### 3.1 Effect of soil permeability on measured sand acceleration

The measured acceleration response of sand in case 1 (water, 200 Gal) and case 5 (Polymer-0.05%, 200 Gal) are shown in Fig. 5. It can be seen that, without liquefaction, the acceleration in the soils follows the input motion at the shaking table base during the first one or two cycles of shaking. It became irregular with changes of amplitudes as the liquefaction occurred in sand specimen and there were some large amplitude spikes as sand liquefied, especially at a shallower depth ($z = 75$ mm and $z = 225$ mm). The similar phenomenon was observed in cases of sloping sand layers and was also reported by other researchers (Taboada *et al.* 1998, Okamura *et al.* 2001). These spikes could be explained by a strength increase in the saturated sand due to the dilative stress-strain response in part of the cycle. It is worth noting that the amplitudes of spikes were comparatively larger and the duration time of spike appears was longer in Case 5 than in Case 1 due to the low
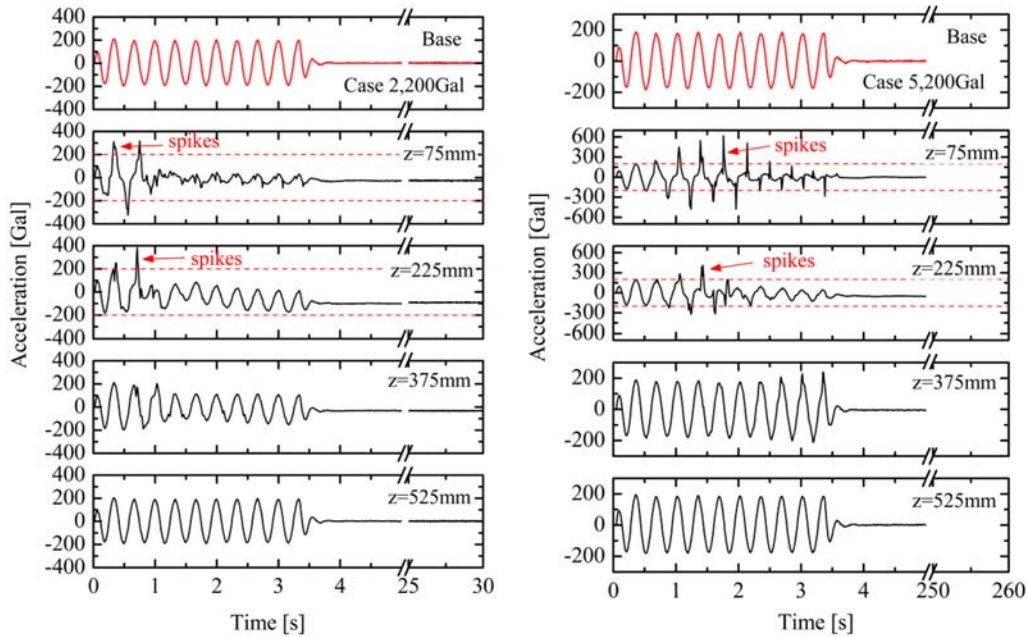


Fig. 5 Acceleration response in Case 2 (water) and Case 5 (Polymer-0.05%)

permeability of sand deposits.

## 3.2 Effect of soil permeability on excess pore pressure dissipation

Fig. 6 compares the excess pore pressure ratios measured in Case 2 (water) and Case 5 (Polymer-0.05%), with both tests having an input peak acceleration of 300 Gal for 2 seconds. The red broken horizontal lines in Fig. 6 indicate the condition of sand liquefaction. It shows clearly the effect of soil permeability on pore pressure dissipation during or after shaking. Excess pore pressure stays to unity for a much longer time in Case 5, which use polymer as pore fluid. By comparison, it starts to decrease rapidly after a few seconds of sand liquefaction in Case 2. In Case 2 and Case 5, the time of excess pore pressure fully dissipated was about 20 seconds and 250 seconds after shaking in each test. It means that liquefaction could remain a longer time when the sand permeability decreases.
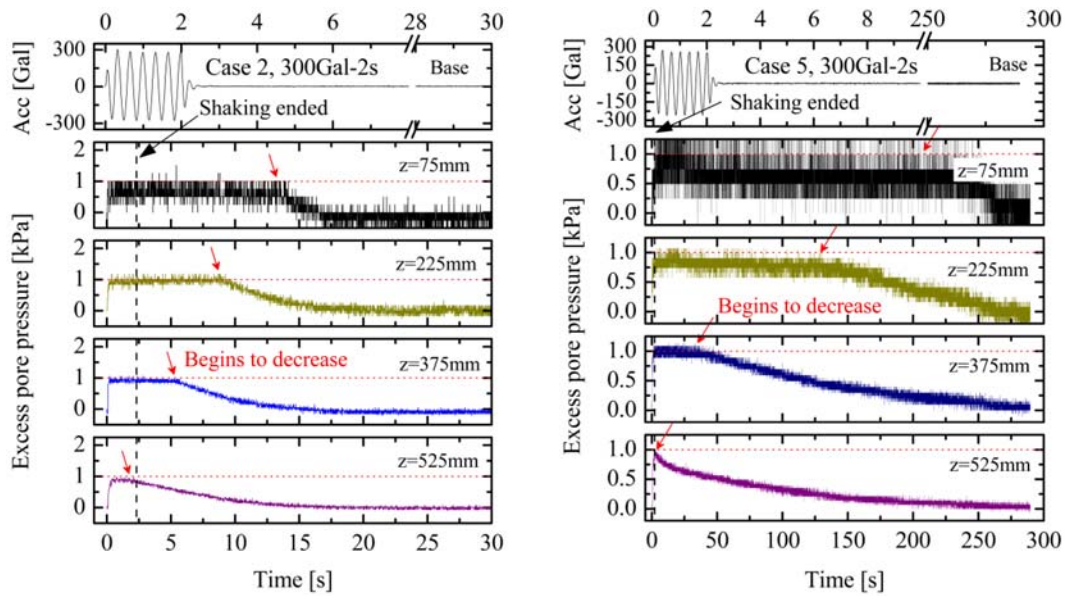
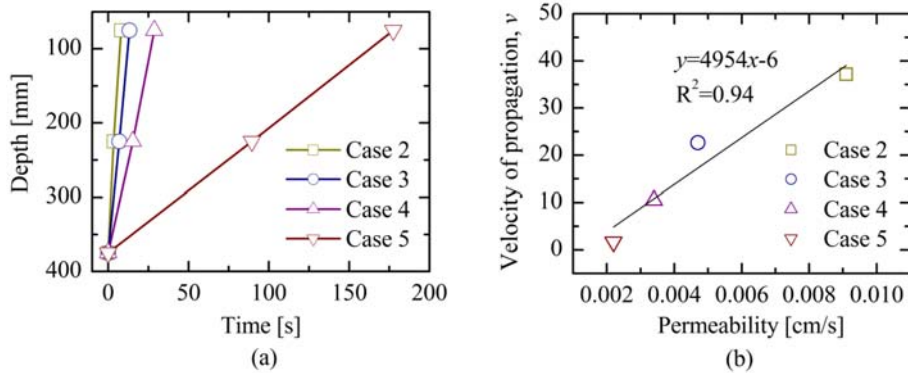Fig. 6 Excess pore pressure in Case 2 (water) and Case 5 (Polymer-0.05%)

Fig. 7 Excess pore pressure dissipation in liquefied sand layer

As illustrated in Fig. 6, showing with small red arrows, the dissipation of excess pore pressures starts from a rather deeper depth and it moves up until it reaches the ground surface. Fig. 7(a) was constructed by taking those times of the pore pressure begins to decrease at different depth based on the excess pore pressure response in Case 2-Case 5, which means the passage time of the liquefied/nonliquefied boundary at each depth (Okamura *et al.* 2001). It can be seen that the elapsed time increased linearly with decreasing depth, and the inclination of lines, which means the velocity of this propagation, have a good proportion to the sand permeability in these tests as shown in Fig. 7(b).

### 3.3 Drainage period characteristic of excess pore pressure

A typical curve showing the generation and dissipation of excess pore pressure during earthquake-induced liquefaction is presented in Fig. 8. In the part where $t > 0$, as shown in Fig. 8, the excess pore pressure, $u(t)$, dissipates roughly according to a negative exponential function (De Groot *et al.* 2006).

$$u(t) \approx u(0) \cdot \exp\left(-\frac{t}{T_{drain}}\right) \tag{9}$$

Where $T_{drain}$ is the drainage period characteristic of excess pore pressure in sand deposit. The value of $T_{drain}$ is mainly determined by the compressibility and permeability of sand and the drainage distance of excess pore pressure flows to the surface.

Based on the theory of soil consolidation, the following expression of $T_{drain}$ can be yielded

$$T_{drain} = \frac{d^2}{c_v} \tag{10}$$

Where $d$ is the drainage distance; $c_v = k/(\gamma_w \cdot m_v)$ is the elastic consolidation coefficient, with $\gamma_w$ is unit weight of the pore fluid; $m_v$ coefficient of volume compressibility. With $d = 60$ cm, $m_v \approx 0.5 \times 10^{-3}$ m$^2$/kN, the following value of $T_{drain}$ in each cases of model tests can be obtained as shown in Fig. 9. The dissipation of excess pore pressure can be roughly described by this method. It also interesting to correlate $T_{drain}$ with the settlement and lateral displacement of liquefied ground discussed later, to consider about the permeability or drainage effect on liquefaction-induced ground deformation.
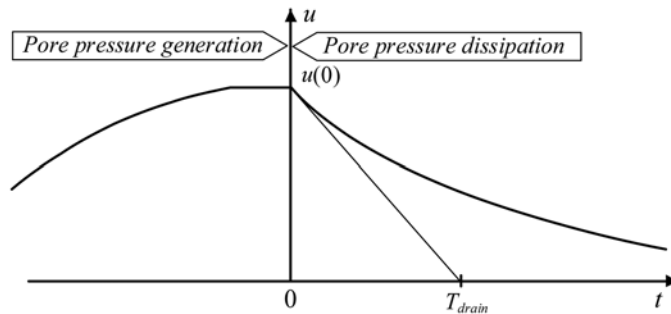


Fig. 8 Excess pore pressure generation and dissipation during liquefaction occurs in sand deposit
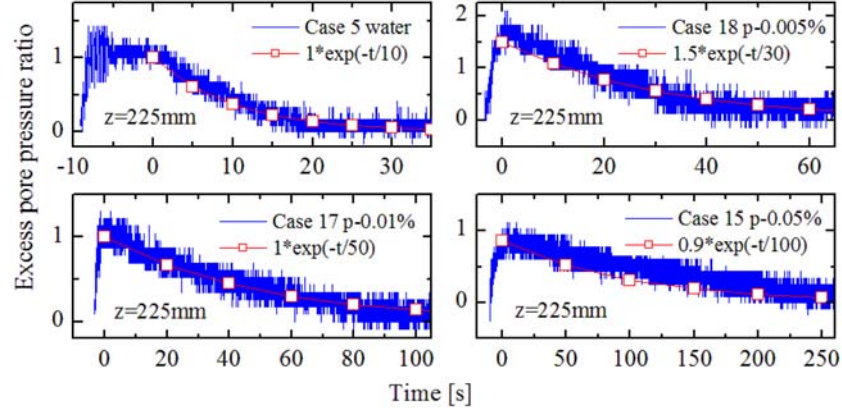
Fig. 9 Excess pore pressure dissipation during liquefaction in sand deposit

## 4. Effects of excess pore pressure dissipation on liquefaction-induced ground deformation

### 4.1 Effect of excess pore pressure dissipation on settlements

There was essentially no settlements of sand deposits (less than 2 mm) when there was no liquefaction (100 Gal). Significant settlements were induced only when liquefaction occurred. Fig. 10 shows the response of excess pore pressure ratio (EPPR) and settlement (Stm) in Case 2 and Case 5.

As shown in Fig. 10(a), the settlements increased rapidly after the beginning of liquefaction and it can be seen that most of the settlements occurred within the time of shaking in Case 2, which used water as pore fluid. Fig. 11 gives an example of the settlement of ground surface in Case 2, about 87% of the total settlement has been occurred during shaking. By comparison, in Case 5 as shown
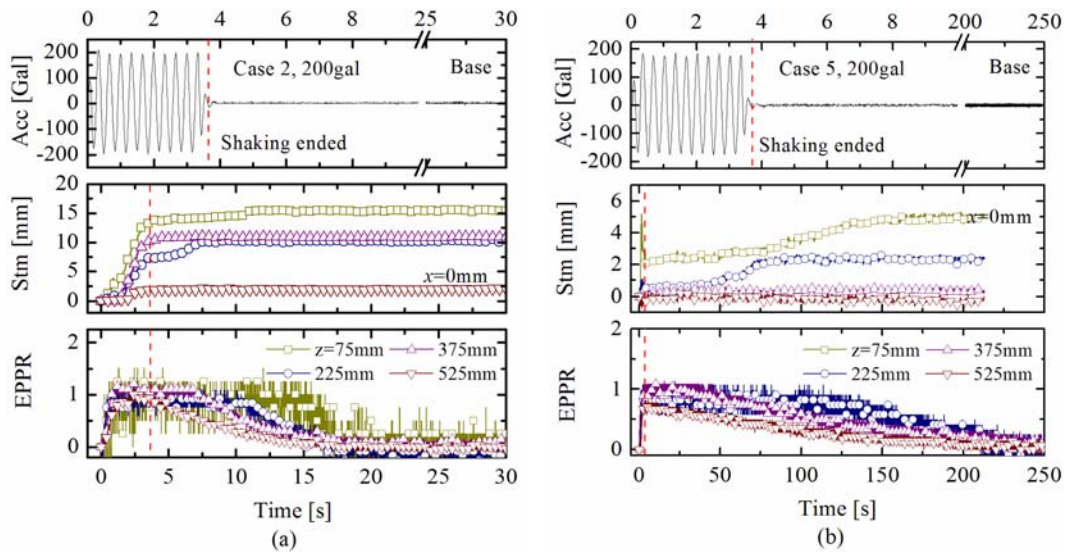


Fig. 10 Excess pore pressure ratio and settlement response in Case 2 (water) and Case 5 (Polymer)
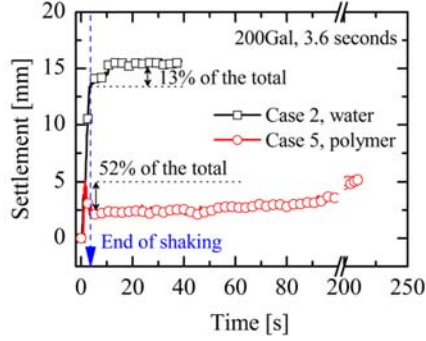
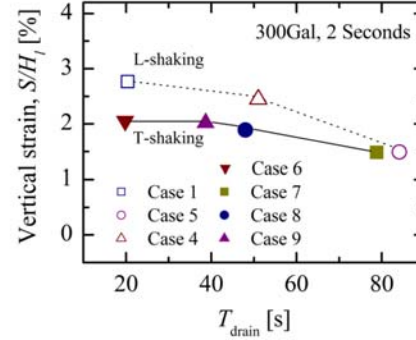Fig. 11 Settlements of sand surface in Case 2 (water) and Case 5 (polymer)

Fig. 12 Settlements of sand surface under 300 Gal for 2 seconds shaking

in Fig. 10(b) and Fig. 11, which used Polymer-0.05% as pore fluid, the settlements continuously increased as the excess pore pressure dissipates after the termination of shaking, and the settlements measured from markers were smaller than in the case that used water as pore fluid. It may suggest that post-liquefaction settlement in the low permeability of sand layer occurs within a more likely static force condition and cause smaller ground settlement in those tests.

Furthermore, the settlements of sand surface measured from Cases of the model test with a level ground, which shown in Fig. 12 are considered under shaking of 300 Gal for 2 seconds. It can be seen that the larger settlements are caused in saturated Toyoura sand deposits with a higher permeability in those model tests. It may indicate that, under dynamic loading, liquefied soil with drainage condition is more effective way to cause densification. The settlement after shaking is mainly due to re-sedimentation of sand particles and redistribution of void within the sand in a low permeability condition.

### 4.2 Effect of excess pore pressure dissipation on lateral flow

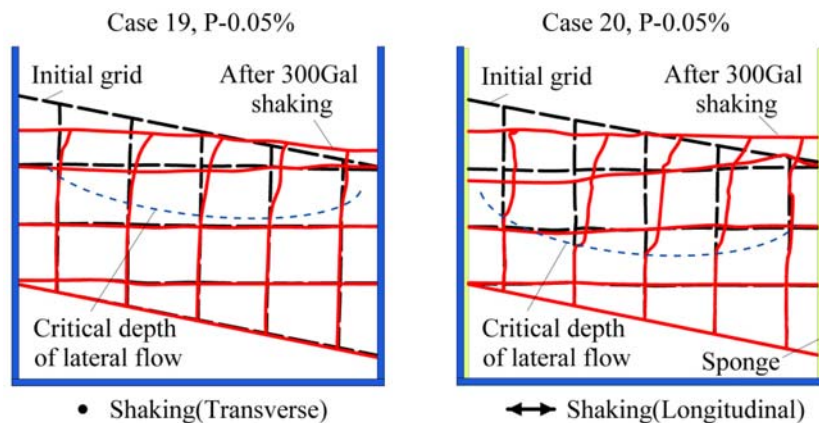Fig. 13 shows an example of the test results, when the gradient of the ground surface is 20% and



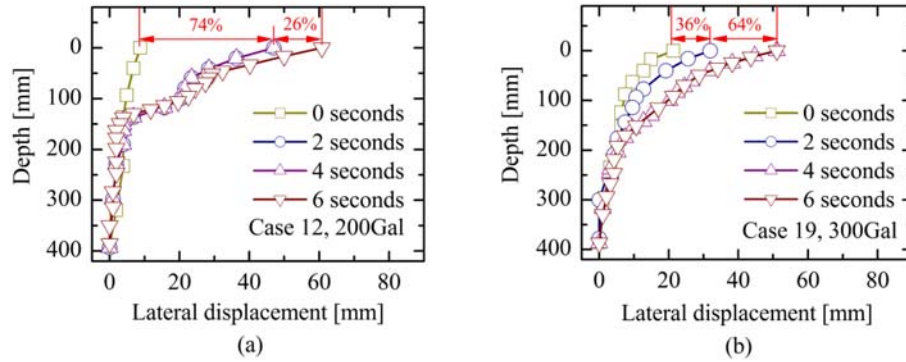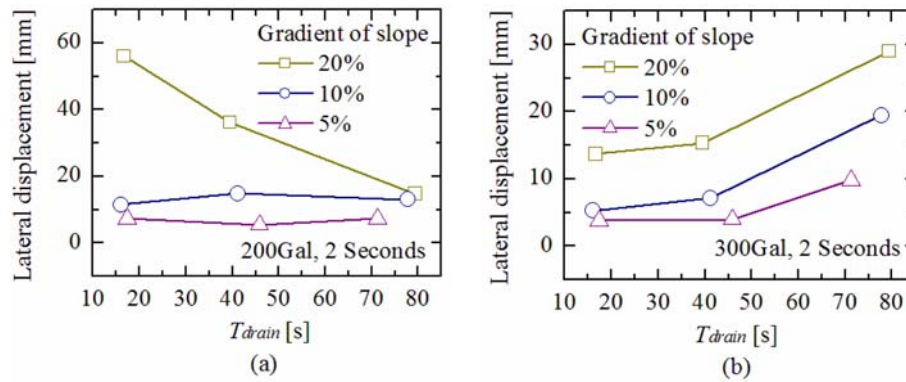Fig. 13 Examples of shaking table test results (Case 19 and Case 20)

Fig. 14 Evolution of lateral displacement with time in Case 12 and Case 19

the pore fluid is polymer-0.05%. The shapes of the grid before and after liquefaction are demonstrated by dashed and solid lines respectively. It is further interesting to note that when shaking is in the same direction with the slope inclination, lateral flow reaches a greater depth than the case in which the shaking is applied perpendicularly to the direction of slope inclination.

According to lateral displacement observations in this study, Fig. 14 shows the evolution of the lateral displacement profiles in Case 12 (200 Gal, 2 seconds) and Case 19 (300 Gal, 2 seconds). The lateral displacement approximately stopped as soon as the shaking ended in both cases, not a matter of the difference of sand permeability. It was different between the processes of settlement and lateral displacement occurred in model tests with low sand permeability by using polymer fluid. As mentioned before, In Case 12, saturated by water with a high permeability of sand, the lateral displacement is a little bit faster than that in Case 19, of which the shaking is stronger.

Although the lateral movement mostly stopped as soon as the shaking ended, when the sand permeability effect on the liquefaction-induced lateral flow are considered, as drawn in Fig. 15(a), the lateral displacement is significantly affected by the permeability of liquefied layer when the gradient of ground surface is 20% in those model tests. Larger lateral displacement occurred in the higher permeability condition, despite the fact that the excess pore pressure did not dissipate until much later. However, this tendency was not clear when the gradient of ground surface is small. Furthermore, Fig. 15(b) shows the ground lateral displacement caused by the followed 300 Gal



Fig. 15 Relationship between lateral displacement and $T_{drain}$

shaking in each model test. It shows that the following shaking will cause much larger lateral displacement in the low permeability sand deposits.

In Fig. 15, it also can be seen that the lateral displacement increased with the gradient of liquefied layer as expected based on previous test results as reported by other researchers (Hamada *et al.* 1998). The relationship between gradient of sand layer and lateral displacement was also affected by the permeability.

## 5. Conclusions

On the basis of these cases of shaking table tests, the following conclusions were drawn;

(1) The acceleration records in sand deposits become irregular as the liquefaction occurs and large amplitude spikes is observed during sand liquefaction. The amplitude and the duration time of spikes appear seem to increase as sand permeability decreases.

(2) Dissipation of excess pore pressure starts from rather deeper depth in both low and high permeability sand. The boundary between the upper liquefied layer and the lower solidified layer moves upward at a constant speed, which increases linearly with the sand permeability.

(3) In the high permeability of sand layer, most of the ground settlement is developed during shaking and does not increase just after the end of shaking. While in the low permeability of sand layer, the settlement continues for a longer time with the dissipation of the excess pore pressure. It seems that larger settlement will be caused in sand layer with the higher permeability.

(4) The lateral displacement of sand layer is mostly developed during shaking in both low and high permeability of sand layers. However, in those model tests, the permeability effect on the lateral displacement becomes significant in liquefied layer with large ground surface gradient and the fallowed shaking will cause large lateral movement in the low permeability sand layer.

## References

De Groot, M.B., Bolton, M.D., Foray, P., Meijers, P., *et al.* (2006), "Physics of liquefaction phenomena around marine structures", *J. Waterw., Port, Coastal, Ocean Eng.*, **132**(4), 227-243.

Dewoolker, M.M., Ko, H.-Y., Stadler, A.T. and Astaneh, S.M.F. (1999), "A substitute pore fluid for seismic centrifuge modeling", *Geotech. Testing J., ASTM*, **22**(3), 196-210.

Yasuda, S., Nagase, H., Kiku, H. and Uchida, Y. (1992), "The mechanism and a simplified procedure for the analysis of permanent ground displacement due to liquefaction", *Solids Found.*, **32**(1), 149-160.

Hamada, M., Yasuda, S. Isoyama, R. and Emoto, K. (1986), "Study on liquefaction induced permanent ground displacements", Association for the development of earthquake prediction.

Hamada, M. and Wakamatsu, K. (1998), "A study on ground displacement caused by soil liquefaction", *Collected Papers of Japan Society of Civil Engineers*, **3**(6), 189-208. (in Japanese)

Lin, M.L. and Wang, K.L. (2006), "Seismic slope behavior in a large-scale shaking table model test", *Engineering Geology*, **86**, 118-133.

Susumu, I. (1989), "Similitude for shaking table tests on soil-structure-fluid model in 1g gravitational field", *Solids Found.*, **29**(1), 105-118.

Iai, S. (1989), "Similitude for shaking table tests on soil-structure-fluid model in 1g gravitational field", *Solids Found.*, **29**(1), 105-118.

Ikeno, K., Mitou, M., Zen, K., Sugano, T. and Nakazawa, H. (2011), "Countermeasure against lateral flow of liquefiable runway ground", *Journal of Japan Society of Civil Engineers*, **67**, 130-144. (in Japanese)

Okamura, M., Abdoun, T.H., Dobry, R. and Sharp, M.K. (2001), "Effects of sand permeability and weak aftershocks on earthquake-induced lateral spreading", *Solids Found.*, **41**(6), 63-77.

Sasaki, Y., Towhata, I., Tokida, T. and Yamada, K. (1992), "Mechanism of permanent displacement of ground caused by seismic liquefaction", *Solids Found.*, **32**(1), 79-96.

Shamoto, Y., Zhang, J.-M. and Goto, S. (1997), "Mechanism of large post-liquefaction deformation in saturated sand", *Solids Found.*, **37**(2), 71-80.

Tomi, Y. (2010), "Study on the optimum rubble mound dimension under composite type breakwater considering wave-induced liquefaction", *Master Thesis Submitted to Kyushu University.*

Toyota, H., Towhata, I., Imamura, S. and Kudo, K. (2004), "Shaking table tests on flow dynamic in liquefied slope", *Solids Found.*, **44**(5), 67-84.

Towhata, I., Orense, R.P. and Toyota, H. (1999), "Mathematical principles in prediction of lateral ground displacement induced by seismic liquefaction", *Solids Found.*, **39**(2), 1-19.

Tohno, I. and Shamoto, Y. (1986), "Liquefaction damage to the ground during the 1983 Nihonkai-Chubu earthquake in Aomori Prefecture", *Natural Disaster Science*, **8**(1), 85-116.

Toboada, V. and Dobry R. (1998), "Centrifuge modeling of earthquake-induced lateral spreading in sand", *ASCE J. of Geotech. and Geoenviromental Engrg.*, **124**(12), 1195-1205.

*CC*